

## Proposal of new ground-motion prediction equations for elastic input energy spectra

Yin Cheng, Andrea Lucchini and Fabrizio Mollaioli\*

*Department of Structural and Geotechnical Engineering, Sapienza University of Rome,  
Via Gramsci 53, Rome, Italy*

*(Received February 27, 2014, Revised May 10, 2014, Accepted May 29, 2014)*

**Abstract.** In performance-based seismic design procedures Peak Ground Acceleration (PGA) and pseudo-Spectral acceleration ( $S_a$ ) are commonly used to predict the response of structures to earthquake. Recently, research has been carried out to evaluate the predictive capability of these standard Intensity Measures (IMs) with respect to different types of structures and Engineering Demand Parameter (EDP) commonly used to measure damage. Efforts have been also spent to propose alternative IMs that are able to improve the results of the response predictions. However, most of these IMs are not usually employed in probabilistic seismic demand analyses because of the lack of reliable Ground Motion Prediction Equations (GMPEs). In order to define seismic hazard and thus to calculate demand hazard curves it is essential, in fact, to establish a GMPE for the earthquake intensity. In the light of this need, new GMPEs are proposed here for the elastic input energy spectra, energy-based intensity measures that have been shown to be good predictors of both structural and non-structural damage for many types of structures. The proposed GMPEs are developed using mixed-effects models by empirical regressions on a large number of strong-motions selected from the NGA database. Parametric analyses are carried out to show the effect of some properties variation, such as fault mechanism, type of soil, earthquake magnitude and distance, on the considered IMs. Results of comparisons between the proposed GMPEs and other from the literature are finally shown.

**Keywords:** elastic input energy spectra; ground motion prediction equation, performance-based earthquake engineering; mixed-effects model

---

### 1. Introduction

In Performance-Based Earthquake Engineering (PBEE) the intensity of the earthquake is quantified through a parameter that is usually denoted as Intensity Measure (IM). A Ground Motion Prediction Equation (GMPE) is an equation for calculating the IM value as a function of different variables representative of the earthquake properties, such as, magnitude, fault mechanism, source-to-site distance and soil condition. The GMPE is a tool commonly used in Probabilistic Seismic Hazard Analysis (PSHA). It gives, in fact, a prediction of the expected (mean) value and standard deviation of the IM at a site, and thus can be used to calculate the annual rate of exceeding a specific earthquake intensity level of interest.

---

\*Corresponding author, Professor, E-mail: [fabrizio.mollaioli@uniroma1.it](mailto:fabrizio.mollaioli@uniroma1.it)

In the literature, many different IMs can be found. Those that have been more largely investigated and that are most commonly used both in PSHA and Probabilistic Seismic Demand Analysis (PSDA) to predict the response of structures to earthquake are the following: the Peak Ground Acceleration (PGA), the Peak Ground Velocity (PGV), the Peak Ground Displacement, and the pseudo-Spectral acceleration ( $S_a$ ). However, studies (e.g., Yakut and Yilmaz 2008; Jayaram *et al.* 2010; Lucchini *et al.* 2011 and 2013; Mollaioli *et al.* 2013) have recently evaluated these IMs and demonstrated the reduced predictive capabilities they have with respect to some types of structures and Engineering Demand Parameters (EDPs) commonly used to measure damage. It is also for such a reason that the interest in studying alternative IMs has been recently renewed.

Several studies proposing energy-based concepts for the definition of earthquake IMs have been carried out in the past (e.g., Akiyama 1985; Uang and Bertero 1990; Decanini and Mollaioli 1998, 2001; and the most recent Takewaki 2004; Kalkan and Kunnath 2008; Benavent-Climent *et al.* 2010a,b; Takewaki and Tsujimoto 2011; and Mollaioli *et al.* 2011). Among the different energy-based parameters that have been studied, the relative and absolute elastic input energy, and the corresponding equivalent velocities, have been found to be good predictors of seismic demand in structures. The good predictive capabilities of these parameters are due to their dependence on amplitude, frequency content and duration of the motion, and on the properties of the structure as well. Input energy has been shown to be a stable parameter of structural response and an effective tool in seismic design (Fajfar and Fischinger 1990; Uang and Bertero 1990). It can be related to the hysteretic energy dissipated by the structure (Decanini and Mollaioli 2001), which is a parameter that is a direct measure of structural damage and considered to be suitable for energy-based seismic design methods (Manfredi 2001). Elastic input energy can be used to predict seismic demand in structures not only in the elastic range of response. It has been shown, in fact, that elastic input energy is also well correlated to the nonlinear response of structures (e.g., see the work of Mollaioli *et al.* 2011 on multistory buildings). In addition, elastic input energy spectra can be used to derive intensity measures that can explicitly account for higher modes contribution (e.g., see the vector IMs studied in Luco *et al.* 2005) and for the elongation of periods of vibration due to damage (e.g., see the integral IMs considered in Mollaioli *et al.* 2013).

Recently, due to increased number of strong motion records available, new GMPEs have been proposed. Many of them have been developed in the Next Generation Attenuation (NGA) project for predicting ground motions from shallow crustal earthquakes in active seismic regions. Details about these new NGA GMPEs can be found in Abrahamson and Silva (2008), Boore and Atkinson (2008), Campbell and Bozorgnia (2008), Chiou and Youngs (2008), and Idriss (2008). These GMPEs have been developed using a ground motion database larger than those used in the past, and advanced functional forms requiring many input variables, namely, many information on the earthquake properties. The IMs predicted by these GMPEs are PGA, PGV, and  $S_a$  only. Studies that recently focused on energy-based intensity measures are really a few. Among them deserve to be mentioned those of Chapman (1999), Gong and Xie (2005), and Danciu and Tselentis (2007). In these studies, GMPEs for input energy equivalent velocities are developed, but only for specific seismic regions and by using a small number of strong ground motion data (due to the available databases at the time they have been proposed). In particular, 304 records from 23 earthquakes occurred in western North America, 266 records from 15 earthquakes in California, and 335 records from 151 Greek earthquakes are used in Chapman (1999), Gong and Xie (2004), and

Danciu and Tselentis (2007), respectively. In these GMPEs very limited consideration is given to site effects, and dummy variables are usually used to represent site classes and soil conditions. Only in Danciu and Tselentis (2007) fault mechanism effects are taken into account in the development of the prediction equations.

The aim of this study is to establish new GMPEs for the absolute and the relative elastic input energy equivalent velocities. In particular, the interest is in the prediction of the geometric mean of the input energy equivalent velocities of the two horizontal components of the ground motion. The equations will be derived using a large set of strong ground motions selected from the NGA database. Improvements with respect to the GMPEs currently available in the literature will be obtained by accounting for the effects of both fault mechanism and soil condition. The latter will not be evaluated with dummy variables but the commonly used parameter  $V_{S30}$ , namely, the value of the average shear-wave velocity between 0 and 30-meters depth. A mixed-effects model for considering the variation of records within-event and between-events (Abrahamson and Youngs 1992) will be employed in the regression analyses for the development of the prediction equations.

## 2. Strong motion database

The NGA database ([http://peer.berkeley.edu/peer\\_ground\\_motion\\_database/site](http://peer.berkeley.edu/peer_ground_motion_database/site)) includes a very large number of strong ground motions recorded worldwide from shallow crustal earthquakes in active tectonic regions. This database, which has already been used by other researchers to develop GMPEs, provides records with comprehensive meta-data (such as earthquake source data and various site characterizations) that enable to constrain relatively complex functional forms for many different earthquake properties (e.g., fault mechanism and  $V_{S30}$ ).

The subset of records selected from the NGA database and used to derive the proposed GMPEs consists of 1550 ground motions from 63 main shock earthquakes. Each of them represents a free-field motion, has two horizontal components and is characterized by a measured or estimated  $V_{S30}$ . The same general criteria used in Campbell and Bozorgnia (2008) to select records to derive prediction equations for the geometric mean horizontal component of PGA, PGV and  $S_a$  is applied. In particular, only earthquakes located within the shallow continental crust in a tectonically active region are selected. All data are from recordings at or near ground level and exhibits no known embedment or topographic effects. In addition, earthquakes having not enough records to reliably represent the mean horizontal ground motion in relation to their magnitude are excluded. The distribution of the selected ground motions with respect to moment magnitude (in the range from 4.26 to 7.9) and site-rupture closest distance (varying from 0.1km to 199.3km) is shown in Fig. 1. In Table 1, a summary of these earthquakes is also reported.

Table 1 Main shock earthquakes used in the study (In the Table, symbols are used with the following meanings: in the Fault Type column, SS, R, RO, N and NO denote Strike-Slip, Reverse, Reverse-Oblique, Normal and Normal-Oblique, respectively; R indicates the closest distance to rupture;  $V_{S30}$  is the average shear-wave velocity between 0 and 30-meters depth; letters A, B, C, D and E indicate different types of soil according to the NEHRP site classification based on the preferred  $V_{S30}$  values.)

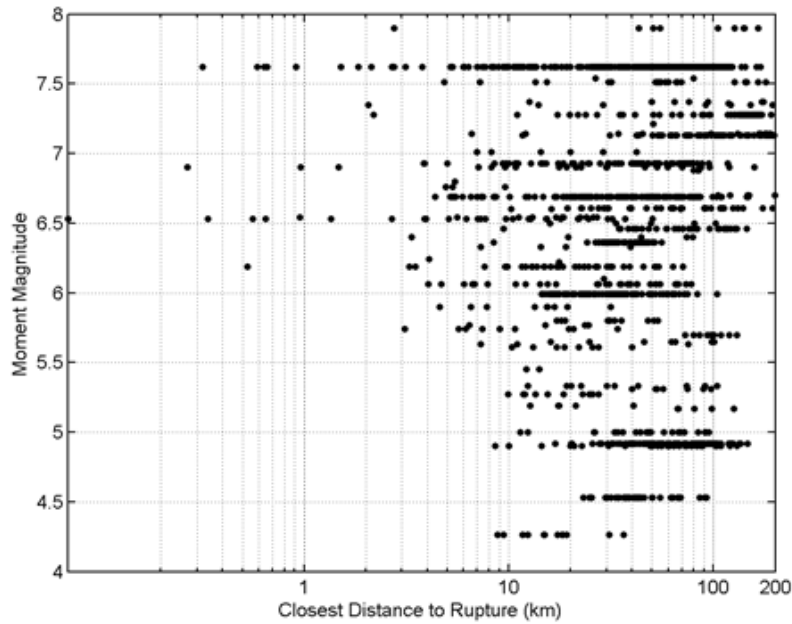


Fig. 1 Magnitude-distance distribution of ground motions used in the study

Table 1 Main shock earthquakes used in the study (In the Table, symbols are used with the following meanings: in the Fault Type column, SS, R, RO, N and NO denote Strike-Slip, Reverse, Reverse-Oblique, Normal and Normal-Oblique, respectively; R indicates the closest distance to rupture;  $V_{S30}$  is the average shear-wave velocity between 0 and 30-meters depth; letters A, B, C, D and E indicate different types of soil according to the NEHRP site classification based on the preferred  $V_{S30}$  values

Earthquake Name	Year	M	Fault Type	Depth (km)	R (km)		$V_{S30}$ (m/s)		Number of recordings				Total No.
					Min.	Max.	Min.	Max.	A+	B	C	D	
Kern County	1952	7.36	R	16	8	117.8	316.5	316.5	0	0	1	0	1
Parkfield	1966	6.19	SS	10	9.6	17.6	256.8	527.9	0	2	2	0	4
Lytle Creek	1970	5.33	RO	8	12.4	103.6	302.0	813.5	1	7	2	0	10
San Fernando Managua.	1971	6.61	R	13	19.3	193.9	235.0	821.7	2	19	12	0	33
Nicaragua-01	1972	6.24	SS	5	4.1	4.1	288.8	288.8	0	0	1	0	1
Friuli. Italy-01	1976	6.5	R	5.1	15.8	102.2	274.5	659.6	0	3	2	0	5
Gazli. USSR	1976	6.8	R	18.2	5.5	5.5	659.6	659.6	0	1	0	0	1
Tabas. Iran	1978	7.35	R	5.75	2.1	194.6	274.5	766.8	1	2	4	0	7
Coyote Lake	1979	5.74	SS	9.6	3.1	33.8	221.8	1428.0	1	5	4	0	10
Norcia. Italy	1979	5.9	N	6	4.6	31.4	338.6	1000.0	1	1	1	0	3
Imperial Valley-06	1979	6.53	SS	9.96	0.1	50.1	162.9	659.6	0	2	30	1	33
Livermore-01	1980	5.8	SS	12	17.2	53.4	271.4	517.1	0	2	3	0	5
Anza (Horse Canyon)-01	1980	5.19	SS	13.6	12.7	40.6	329.0	724.9	0	3	2	0	5

Table 1 Continued

Earthquake Name	Year	<i>M</i>	Fault Type	Depth (km)	<i>R</i> (km)		<i>V<sub>s30</sub></i> (m/s)		Number of recordings				Total No.
					Min.	Max.	Min.	Max.	A+B	C	D	E	
Mammoth Lakes-01	1980	6.06	NO	9	4.7	15.5	338.5	370.8	0	1	2	0	3
Victoria. Mexico	1980	6.33	SS	11	7.3	39.3	274.5	659.6	0	1	3	0	4
Irpinia. Italy-01	1980	6.9	N	9.5	8.2	59.6	274.5	1000.0	5	5	2	0	12
Corinth. Greece	1981	6.6	N	7.15	10.3	10.3	338.6	338.6	0	0	1	0	1
Westmorland	1981	5.9	SS	2.3	6.5	19.4	191.1	362.4	0	1	5	0	6
Coalinga-01	1983	6.36	R	4.6	8.4	55.8	184.8	684.9	0	25	20	0	45
Borah Peak. ID-01	1983	6.88	N	16	79.6	84.8	424.8	659.6	0	3	0	0	3
Morgan Hill	1984	6.19	SS	8.5	0.5	70.9	116.4	1428.0	1	10	15	1	27
Lazio-Abruzzo. Italy	1984	5.8	N	14	18.9	51.3	200.0	659.6	0	1	4	0	5
Nahanni. Canada	1985	6.76	R	8	4.9	9.6	659.6	659.6	0	3	0	0	3
Hollister-04	1986	5.45	SS	8.72	12.2	14.1	215.5	684.9	0	1	2	0	3
N. Palm Springs	1986	6.06	RO	11	4.0	78.1	207.5	684.9	0	13	18	0	31
Chalfant Valley-01	1986	5.77	SS	6.7	6.4	24.5	271.4	345.4	0	0	5	0	5
Chalfant Valley-02	1986	6.19	SS	10	7.6	52.0	271.4	359.2	0	0	11	0	11
New Zealand-02	1987	6.6	N	6.4	16.1	68.7	424.8	424.8	0	2	0	0	2
Whittier Narrows-01	1987	5.99	RO	14.6	14.5	103.9	160.6	1222.5	3	49	56	1	109
Whittier Narrows-02	1987	5.27	RO	13.3	9.9	27.5	271.9	821.7	1	3	6	0	10
Superstition Hills-01	1987	6.22	SS	10	17.6	17.6	207.5	207.5	0	0	1	0	1
Superstition Hills-02	1987	6.54	SS	9	1.0	27.0	191.1	362.4	0	1	10	0	11
Loma Prieta	1989	6.93	RO	17.4 8	3.9	117.1	116.4	1428.0	7	37	28	5	77
Griva. Greece	1990	6.1	N	9.45	29.2	29.2	338.6	338.6	0	0	1	0	1
Erzican. Turkey	1992	6.69	SS	9	4.4	4.4	274.5	274.5	0	0	1	0	1
Cape Mendocino	1992	7.01	R	9.6	7.0	42.0	311.8	712.8	0	4	2	0	6
Landers	1992	7.28	SS	7	2.2	190.1	207.5	684.9	0	20	47	0	67
Big Bear-01	1992	6.46	SS	13	9.4	144.6	207.5	821.7	1	14	23	0	38
Northridge-01	1994	6.69	R	17.5	5.2	147.6	160.6	2016.1	13	67	68	1	149
Kobe. Japan	1995	6.9	SS	12.6 17.9	0.3	158.6	256.0	609.0	0	4	8	0	12
Kozani. Greece-01	1995	6.4	N	4	19.5	79.4	338.6	659.6	0	2	1	0	3
Dinar. Turkey	1995	6.4	N	5	3.4	44.2	219.8	338.6	0	0	2	0	2
Kocaeli. Turkey	1999	7.51	SS	15	4.8	180.2	175.0	811.0	1	9	11	1	22
Chi-Chi. Taiwan	1999	7.62	RO	6.76	0.3	169.9	124.3	1525.9	7	1	6	7	381
Duzce. Turkey	1999	7.14	SS	10	6.6	188.7	175.0	659.6	0	4	9	1	14
Caldiran. Turkey	1976	7.21	SS	10	50.8	50.8	274.5	274.5	0	0	1	0	1
St Elias. Alaska	1979	7.54	R	15.7	26.5	80.0	274.5	274.5	0	0	2	0	2

Table 1 Continued

Earthquake Name	Year	$M$	Fault Type	Depth (km)	$R$ (km)		$V_{S30}$ (m/s)		Number of recordings				Total No.
					Min.	Max.	Min.	Max.	A+B	C	D	E	
Upland	1990	5.63	SS	4.49	7.3	75.5	229.8	659.6	0	2	1	0	3
Manjil. Iran	1990	7.37	SS	19	12.6	174.6	274.5	724.0	0	1	6	0	7
Sierra Madre	1991	5.61	R	12	10.4	39.8	349.4	996.4	2	5	1	0	8
Little Skull Mtn.NV	1992	5.65	N	12	16.1	100.2	274.5	659.6	0	3	5	0	8
Hector Mine	1999	7.13	SS	5	11.7	198.1	202.9	724.9	0	30	47	0	77
Yountville	2000	5	SS	10.1 2	11.4	94.4	133.1	712.8	0	4	15	5	24
Big Bear-02	2001	4.53	SS	9.1	23.1	92.3	207.5	684.9	0	9	34	0	43
Mohawk Val. Portola	2001	5.17	SS	3.95	66.8	125.8	274.5	345.4	0	0	6	0	6
Anza-02	2001	4.92	NO	15.2	16.8	133.3	196.3	845.4	1	26	45	0	72
Gulf of California CA/Baja Border Area	2001	5.7	SS	10	72.8	130.0	196.3	345.4	0	0	11	0	11
	2002	5.31	SS	7	39.9	97.0	191.1	231.2	0	0	9	0	9
Gilroy	2002	4.9	SS	10.1 2	8.6	130.1	155.4	729.7	0	20	13	1	34
Yorba Linda	2002	4.26	SS	7	8.8	36.3	270.2	376.1	0	7	5	0	12
Nenana Mountain. Alaska	2002	6.7	SS	4.2	104. 7	199.3	274.5	659.6	0	4	1	0	5
Denali. Alaska	2002	7.9	SS	4.86	2.7	164.7	274.5	963.9	2	4	3	0	9
Big Bear City	2003	4.92	SS	6.3	25.5	146.2	207.5	684.9	0	12	24	0	36

### 3. Elastic input energy equivalent velocities

For an elastic damped SDOF (Single-Degree-Of-Freedom) system subjected to ground acceleration  $\ddot{x}_g$ , the equation of motion can be simply written as follows

$$m\ddot{x} + c\dot{x} + kx = -m\ddot{x}_g \quad (1)$$

where  $m$ ,  $c$  and  $k$  are mass, viscous damping coefficient and stiffness of the SDOF, respectively,  $x$  is the relative displacement of the SDOF system with respect to the ground, and  $x_g$  is the ground displacement.

Integrating Eq. (1) with respect to  $x$ , and denoting with  $x_t$  the total displacement of the SDOF system, the two following equations can be derived:

$$\frac{m\dot{x}_t^2}{2} + \int (c\dot{x})dx + \frac{kx^2}{2} = \int m\ddot{x}_t dx_g = E_{Ia} \quad (2)$$

$$\frac{m\dot{x}^2}{2} + \int (c\dot{x})dx + \frac{kx^2}{2} = -\int m\ddot{x}_g dx = E_{Ir} \quad (3)$$

where  $x = x_t - x_g$ . Using Eqs. (2)-(3) two different input energies can be defined (e.g., see Uang and Betero 1990): the absolute input energy  $E_{Ia}$  (i.e.,  $\int m\ddot{x}_t dx_g$  corresponding to the right side term of

Eq. (2)), which is equal to the work done by the total force  $m\ddot{x}_t$  applied to the base of the SDOF system in the ground displacement  $x_g$ , and the relative input energy  $E_{Ir}$  (i.e.,  $-\int m\ddot{x}_g dx$  corresponding to the right side term of Eq. (3)), which is equal to the work done by the equivalent force  $-m\ddot{x}_g$  in the displacement of the SDOF system relative to the ground  $x$ . In order to eliminate the dependence on mass, these two energy parameters can be conveniently converted into equivalent velocities using the following equation:

$$V = \sqrt{2E / m} \tag{4}$$

The maximum value of the velocities through the ground motion duration can be identified, and the absolute and relative input energy spectra can be consequently defined as follows (Akiyama 1985; Uang and Bertero 1990; Kalkan and Kunnath 2008; Takewaki and Tsujimoto 2011):

$$V_{Ela} = \sqrt{2E_{Ia} / m} \tag{5}$$

$$V_{EIr} = \sqrt{2E_{Ir} / m} \tag{6}$$

With the increase of the oscillator period of the SDOF system,  $V_{Ela}$  approaches zero whereas  $V_{EIr}$  points toward the maximum ground velocity. At low oscillator periods, instead,  $V_{EIr}$  approaches zero while  $V_{Ela}$  is asymptotic to the maximum ground velocity. Regardless of the considered oscillator period of the SDOF system,  $E_{Ia}$  and  $E_{Ir}$  converge to almost the same value at the end of the ground motion duration. However, their maximum value (and that of  $V_{Ela}$  and  $V_{EIr}$  as well) is different, and do not usually occur at the end of the ground motion. In particular, for forward-directivity records characterized by distinguishable acceleration pulses the input energy does not accumulate gradually, resulting in instantaneous peaks occurring before the termination of the ground motion (Kalkan and Kunnath 2008). In such cases, if the input energy is evaluated at the end of the ground motion duration, the maximum value may be significantly underestimated.

#### 4. Proposed prediction equations

As already stated in the Introduction, a Ground Motion Prediction Equation (GMPE) is an equation for estimating a ground motion Intensity Measure (IM, which in the case of the present study is  $V_{Ela}$  and  $V_{EIr}$ ) at a given location, once information on source of the earthquake, source-to-site path and site condition are known. Usually, the predictive parameters that are considered in the equation are the earthquake magnitude, the source-to-site distance, and other parameters for characterizing the fault type mechanism and the type of soil. The standard approach to develop a GMPE is to carry out a regression analysis on IM values calculated from a database of earthquake records, by using a fixed- or a mixed-effects model. In statistics, the term “effects” is used to denote the parameters of a predictive model. In fixed-effects models, parameters are assumed to be the same each time data is collected, while in random-effects models they are considered sample-dependent random variables. In mixed-effects models, both fixed and random effects are accounted for; correlations within sample subgroups of data are recognized and represented with additional error terms in the predictive equation. By using a fixed-effects model for the GMPE, the  $k$ -th value of the IM can be expressed as follows:

$$\ln(IM_i) = f(M_i, R_i, \theta) + \varepsilon_i \tag{7}$$

where  $f(M_i, R_i, \theta)$  is a functional form consisting in the ground motion prediction equation,  $M_i$  is the earthquake magnitude of the  $i$ -th record,  $R_i$  is the distance,  $\theta$  is a model coefficient matrix, and  $\varepsilon_i$  is an error term that is usually assumed to be normally distributed with zero mean. The symbol  $\ln$  is used to denote the natural logarithm. The main limit of this type of model is that can lead to bias if the data are not uniformly distributed among the predictor variables, that is, if data are dominated by many records from few earthquakes or recording sites.

In order to overcome this limit and to reduce the bias, a mixed-effects model can be adopted (e.g., see Brillinger and Preisler 1984 and 1985; Abrahamson and Youngs 1992; Özbey *et al.* 2004; Danciu and Tselentis 2007). In this model, the IM value for the  $j$ -th ground motion record from the  $i$ -th earthquake is expressed as follows:

$$\ln(IM_{ij}) = f(M_i, R_{ij}, \theta) + \eta_i + \varepsilon_{ij} \quad (8)$$

where

$M$ ,  $R$  and  $\theta$  denote again magnitude, distance and a model coefficient matrix,  
 $\varepsilon_{ij}$  is the error term for the  $j$ -th ground motion record from the  $i$ -th earthquake,  
 $\eta_i$  is the random effect for the  $i$ -th earthquake.

$\eta_i$  and  $\varepsilon_{ij}$  are assumed to be independent and normally distributed with zero mean and variance equal to  $\tau^2$  and  $\sigma^2$ , respectively. Consequently, the total standard error ( $\sigma_T$ ) for this model is equal to  $\sqrt{\tau^2 + \sigma^2}$ . Using the mixed-effects model, the earthquake-to-earthquake (inter-event) variability resulting from differences in the data recorded from different earthquakes can be accounted for, as well as the within-earthquake (intra-event) variability resulting from differences in data from records at different stations produced by the same earthquake.

In the present work, the following mixed-effects model, calibrated with the NLME (Nonlinear Mixed-Effects model) package implemented in the statistical software R (Pinheiro *et al.* 2007), is employed for deriving the GMPEs:

$$\ln(IM_{ij}) = f(M_i, R_{ij}, V_{S30ij}, NR_i, RS_i, \theta) + \eta_i + \varepsilon_{ij} \quad (9)$$

where

$IM_{ij}$  is the considered IM (i.e.,  $V_{Ela}$  or  $V_{EIr}$ ) value for the  $j$ -th record and the  $i$ -th event,  
 $M_i$  is again the moment magnitude of the  $i$ -th event,  
 $R_{ij}$  is the closest distance to rupture from the  $i$ -th event to the station of the  $j$ -th recording,  
 $V_{S30}$  is the value of the average shear-wave velocity between 0 and 30 meters depth,  
and with the variables NR and RS given as follows  
 $NR=1$  for normal fault mechanism and normal-oblique, 0 otherwise,  
 $RS=1$  for reverse fault and reverse-oblique mechanism, 0 otherwise,  
 $NR=0$  and  $RS=0$  for strike-slip fault mechanism.

The specific functional form used for the prediction of both  $V_{Ela}$  and  $V_{EIr}$  is

$$\begin{aligned} \ln(IM_{ij}) = & a + b(M_i - 6) + c(M_i - 6)^2 + (d + fM_i) \ln \sqrt{R_{ij}^2 + h^2} + e \ln(V_{S30ij} / 1130) \\ & + m1NR_i + m2RS_i + \eta_i + \varepsilon_{ij} \end{aligned} \quad (10)$$

with model coefficients  $a$ ,  $b$ ,  $c$ ,  $d$ ,  $e$ ,  $f$ ,  $m1$ ,  $m2$ , and the ‘fictitious’ focal depth  $h$  used to provide a better fit to the data at short distances (Abrahamson and Silva 1997 ; Özbey *et al.* 2004)

Eq. (10) is a modification of the following functional form

$$\ln(IM_{ij}) = a + b(M_i - 6) + c(M_i - 6)^2 + d \log \sqrt{R_{ij}^2 + h^2} + eG_{ci} + fG_{di} + \eta_i + \varepsilon_{ij} \quad (11)$$

where

$G_{ci}=1$  for site class C, 0 otherwise, and

$G_{di}=1$  for site class D, 0 otherwise,

which has been originally proposed by Boore *et al.* (1993) to study the attenuation of  $S_a$ , and then used by Chapman (1999) and Gong and Xie (2005) to develop prediction equations for the input energy equivalent velocity  $V_{Ela}$  and  $V_{EIr}$ . It can be noted that in Eq. (10) an additional magnitude-dependent slope in the distance term is included. This term, in fact, has been found to be necessary to extend the ground motion model to distances of 200km (e.g., see Campbell and Bozorgnia 2008).  $V_{S30}$  is used to characterize the soil conditions instead of the indicator variables  $G_{ci}$  and  $G_{di}$  of Eq. (11). Studies (e.g., Piggott and Stafford 2012) showed in fact that use of the continuous predictor variable  $V_{S30}$  enables to more adequately capture the site response by eliminating bias of ground motions on the  $V_{S30}$  produced when only dummy variables are considered. Finally, in order to account for fault mechanism effects two other terms (i.e.,  $m1NR$  and  $m2RS$ ) are added at the end of the functional form.

## 5. Regression analyses

The results of the regression analyses carried out to calibrate the model coefficients of  $V_{Ela}$  and  $V_{EIr}$  for a damping value equal to 5% are reported in Tables 2 and 3. In these Tables, the values of the standard error  $\tau$  and  $\sigma$  of the inter-event and intra-event residuals are also given, as well as the obtained total standard error  $\sigma_T$  values. Predictive equations for spectra corresponding to different values of the damping ratio could be developed by recalibrating the regression coefficients. In alternative, damping modification factors (Rezaeian *et al.* 2012) could be eventually developed and used.

Figures from 2 to 5 show for the case of  $V_{Ela}$  the dependence of inter-event and intra-event residuals on magnitude, distance and  $V_{S30}$ . It can be observed that there is no significant trend or bias that results from the use of the considered functional form, confirming the used function to be appropriate for the selected predictor variables. Results of other tests carried out to evaluate the prediction model are reported in Fig. 6. In this Figure, the normal Quantile-Quantile plots for the residuals of  $V_{Ela}$  are reported, showing that both total and intra-event residuals, derived using the established GMPEs, have a very good fit to the assumed normal distribution. Similar results were obtained also for  $V_{EIr}$ .

In Fig. 7, the model coefficients of  $V_{Ela}$  and  $V_{EIr}$  calculated at different period values  $T$  are compared (since the period range 0-2s is of particular interest to low mid-rise buildings, a zoom of these plots in this period range is reported in the Appendix). It can be observed that at periods lower than around 1s, the linear and quadratic magnitude coefficients of the  $V_{Ela}$  and  $V_{EIr}$  functional forms are almost the same. This means that at short periods the scaling of the two velocities with magnitude is very similar. For period values lower than 1.5s, a similar trend can be also observed for the model coefficients  $m1$  and  $m2$ , denoting the same sensitivity of  $V_{Ela}$  and  $V_{EIr}$  on fault mechanism type in this period range. At short periods, distance coefficients  $d$  and  $f$  of the two velocities are nearly the same, but the  $h$  value is higher for  $V_{EIr}$  than for  $V_{Ela}$  indicating faster intensity attenuation for  $V_{EIr}$  than for  $V_{Ela}$ . Independently from the period value, values of the model coefficient  $e$  of  $V_{Ela}$  and  $V_{EIr}$  are very close, implying that site effects for the two velocities

are almost same. About standard errors, the opposite trends can be identified for  $T$  values lower and higher than 1s. In particular, for  $T < 0.5s$  the values of  $\tau$  and  $\sigma$  obtained for  $V_{EIr}$  are significantly higher than those found for  $V_{Ela}$ . On the other hand, for  $T > 2s$  the values of the  $V_{Ela}$  standard errors are higher than those obtained in the  $V_{EIr}$  predictions.

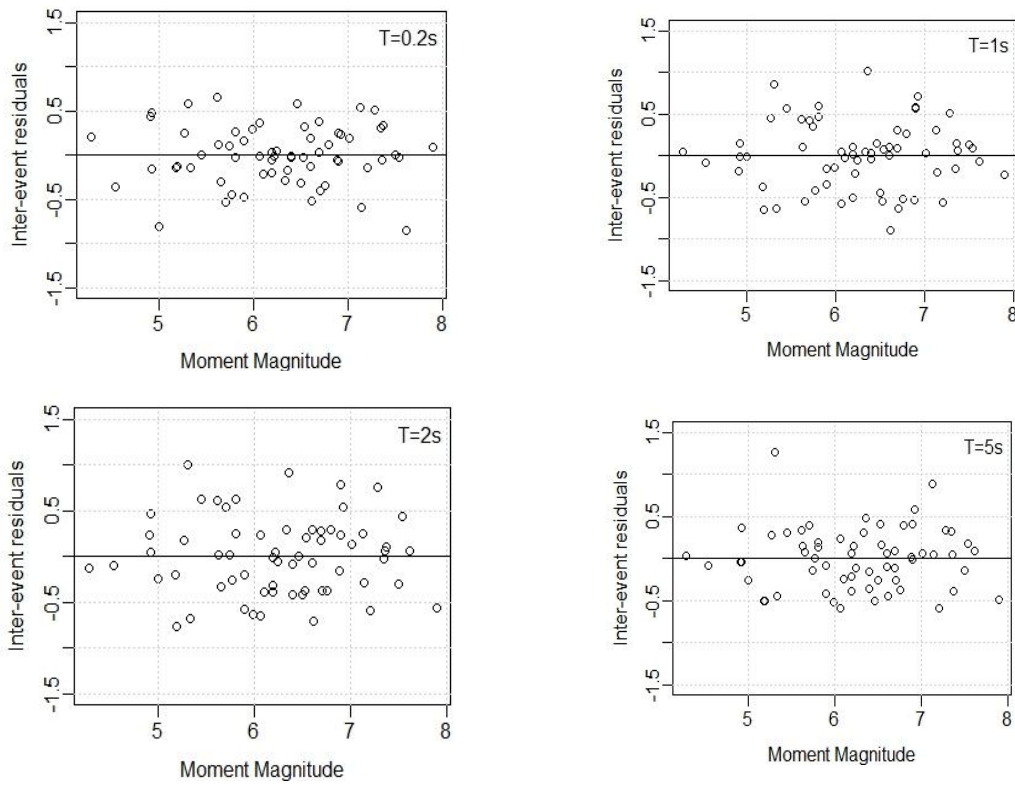


Fig. 2 Dependence of inter-event residuals of  $V_{Ela}$  on moment magnitude

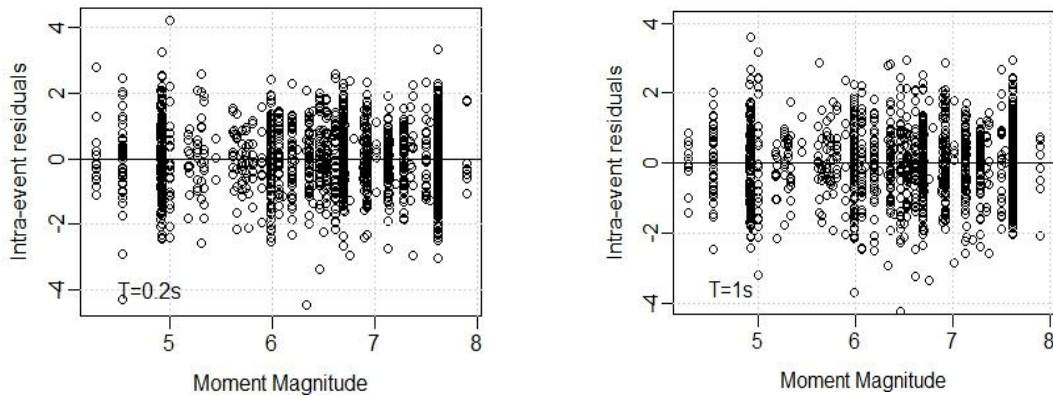


Fig. 3 Continued

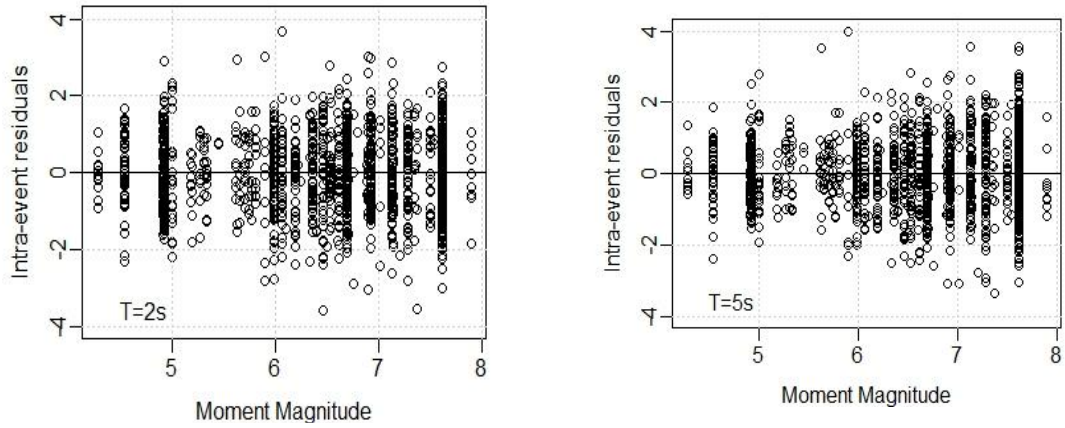


Fig. 3 Dependence of intra-event residuals of  $V_{Ela}$  on moment magnitude

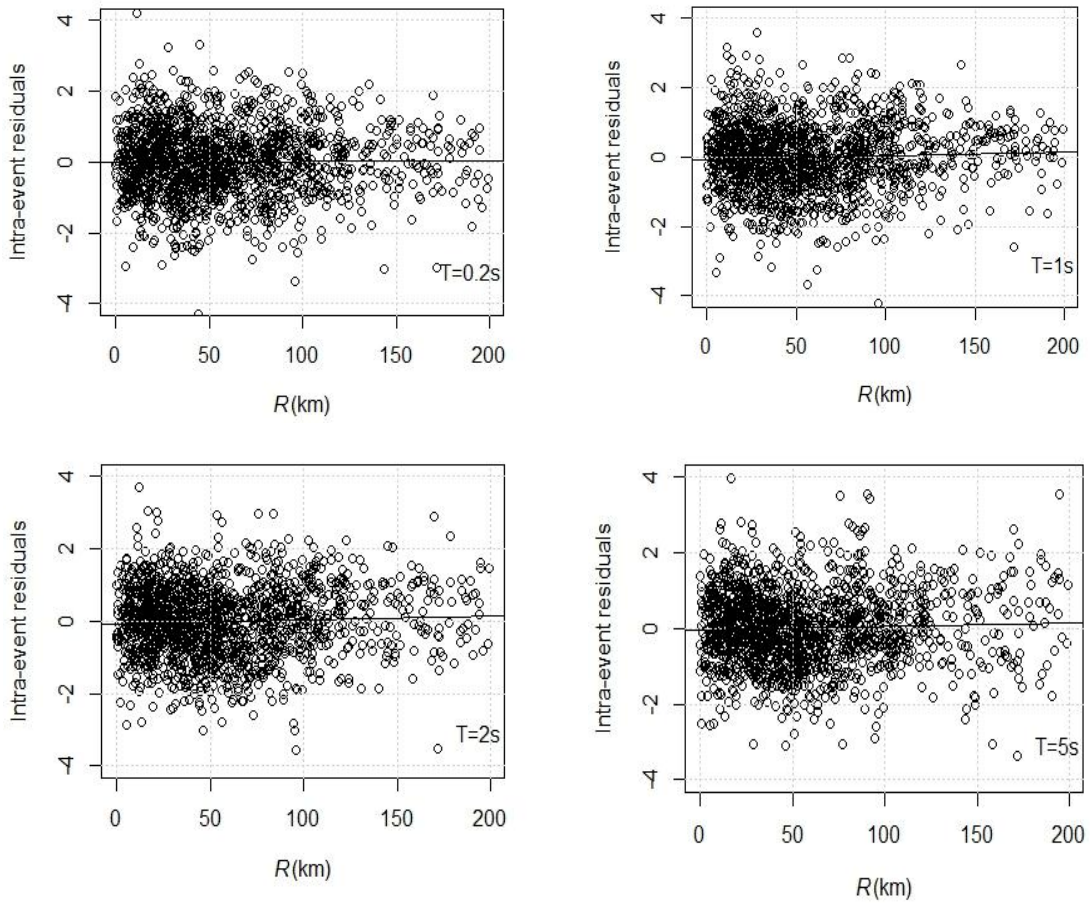


Fig. 4 Dependence of intra-event residuals of  $V_{Ela}$  on rupture distance ( $R$ )

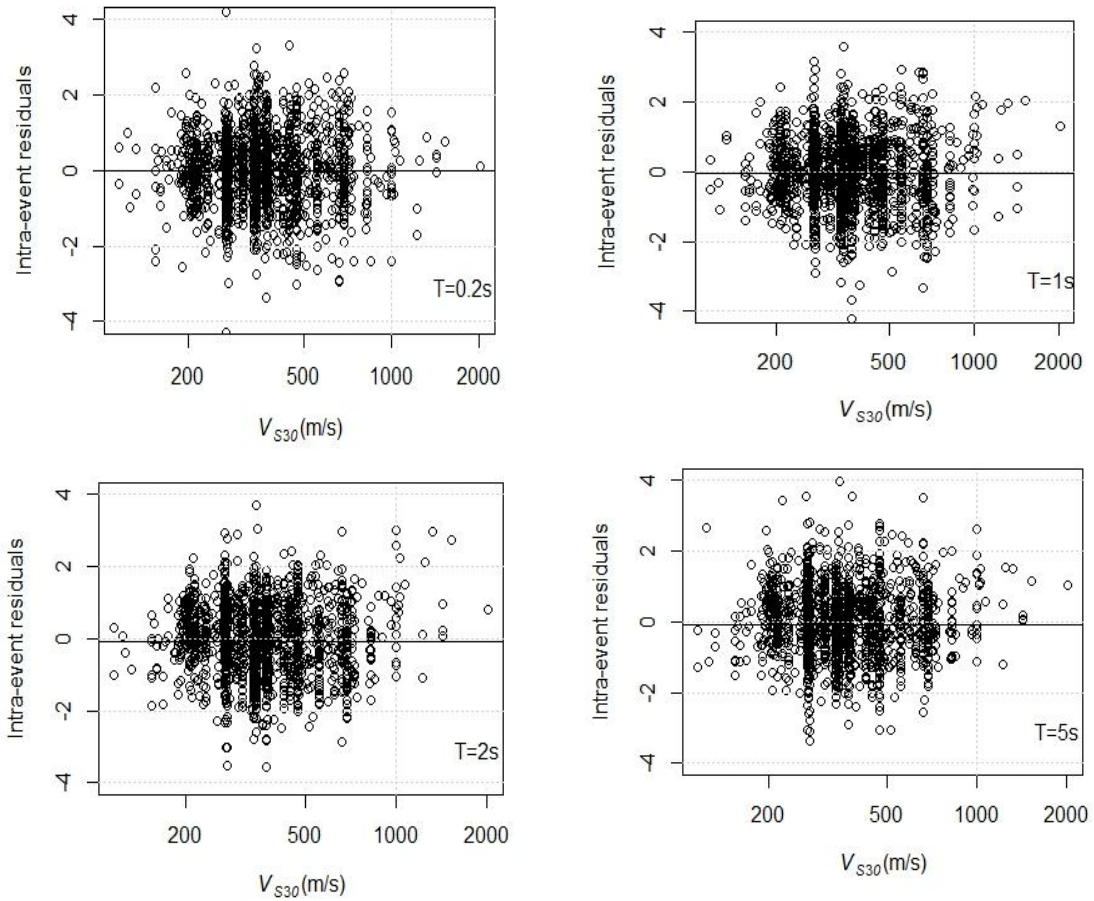


Fig. 5 Dependence of intra-event residuals of  $V_{Ela}$  on  $V_{S30}$

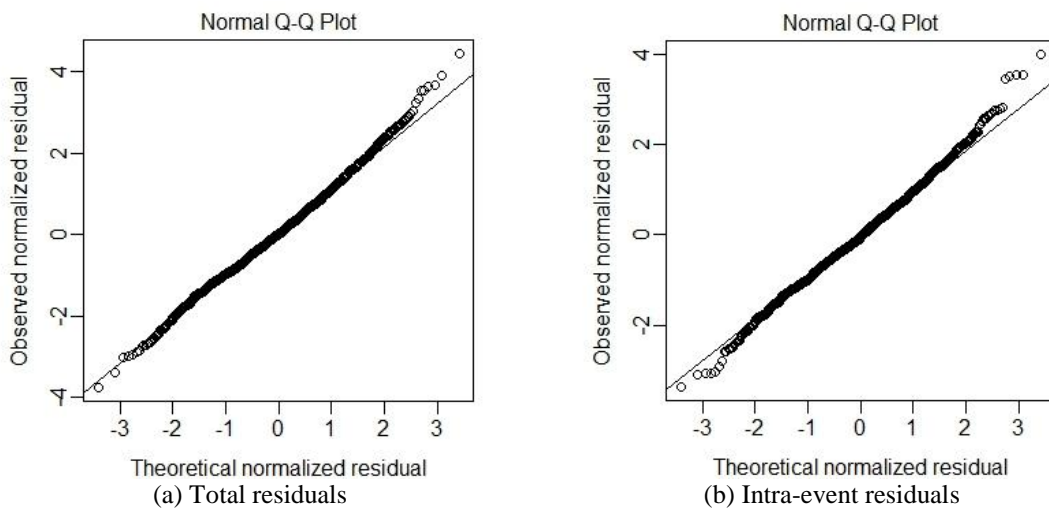


Fig. 6 Normal Q-Q plot for the  $V_{Ela}$  residuals obtained using the proposed GMPE

Table 2 Results of the regression analyses on  $V_{Ela}$  obtained for different values of the SDOF period  $T$

$T[s]$	$a$	$b$	$c$	$d$	$e$	$f$	$h$	$m1$	$m2$	$\tau$	$\sigma$	$\sigma_T$
0.05	4.555	0.423	-0.105	-2.023	-0.465	0.172	3.308	-0.212	0.246	0.209	0.474	0.518
0.1	5.107	0.312	-0.099	-2.023	-0.323	0.168	4.423	-0.079	0.236	0.206	0.452	0.496
0.15	5.531	0.304	-0.111	-1.945	-0.289	0.153	5.884	-0.048	0.228	0.196	0.441	0.483
0.2	5.375	0.569	-0.138	-1.457	-0.316	0.087	6.118	0.011	0.216	0.190	0.439	0.478
0.25	5.337	0.685	-0.159	-1.273	-0.381	0.061	6.135	-0.027	0.203	0.191	0.445	0.484
0.3	5.199	0.737	-0.168	-1.155	-0.443	0.048	5.509	-0.084	0.227	0.202	0.460	0.503
0.35	5.245	0.734	-0.162	-1.187	-0.459	0.053	5.456	-0.130	0.188	0.193	0.472	0.510
0.4	5.296	0.711	-0.156	-1.280	-0.469	0.067	5.499	-0.134	0.172	0.210	0.475	0.520
0.45	5.286	0.697	-0.159	-1.354	-0.511	0.079	5.348	-0.164	0.141	0.221	0.486	0.534
0.5	5.273	0.707	-0.161	-1.380	-0.552	0.083	5.369	-0.203	0.135	0.211	0.496	0.539
0.55	5.188	0.696	-0.176	-1.417	-0.583	0.092	4.910	-0.216	0.141	0.208	0.510	0.551
0.6	5.103	0.691	-0.188	-1.453	-0.612	0.099	4.617	-0.214	0.150	0.221	0.519	0.564
0.65	4.973	0.694	-0.197	-1.458	-0.644	0.104	4.060	-0.202	0.172	0.231	0.527	0.575
0.7	4.890	0.690	-0.197	-1.471	-0.670	0.107	3.509	-0.221	0.198	0.232	0.532	0.580
0.75	4.844	0.707	-0.199	-1.465	-0.688	0.107	3.213	-0.232	0.197	0.232	0.531	0.580
0.8	4.779	0.724	-0.203	-1.460	-0.700	0.107	3.143	-0.212	0.193	0.236	0.530	0.580
0.85	4.751	0.737	-0.209	-1.469	-0.706	0.109	3.099	-0.208	0.185	0.241	0.534	0.586
0.9	4.749	0.732	-0.207	-1.509	-0.715	0.114	3.115	-0.212	0.188	0.253	0.537	0.594
0.95	4.756	0.713	-0.211	-1.571	-0.726	0.124	3.118	-0.230	0.171	0.265	0.539	0.600
1	4.751	0.696	-0.220	-1.632	-0.745	0.133	3.102	-0.245	0.159	0.273	0.541	0.606
1.1	4.702	0.699	-0.242	-1.681	-0.794	0.141	-2.900	-0.299	0.130	0.292	0.544	0.617
1.2	4.679	0.716	-0.254	-1.710	-0.800	0.145	-2.716	-0.325	0.113	0.306	0.546	0.626
1.3	4.633	0.767	-0.253	-1.688	-0.816	0.141	-2.925	-0.390	0.079	0.313	0.548	0.631
1.4	4.573	0.827	-0.243	-1.634	-0.836	0.132	-3.141	-0.441	0.065	0.313	0.547	0.630
1.5	4.527	0.880	-0.236	-1.579	-0.845	0.123	3.338	-0.480	0.052	0.313	0.548	0.631
1.6	4.478	0.918	-0.234	-1.561	-0.852	0.120	3.319	-0.483	0.024	0.311	0.552	0.634
1.7	4.406	0.937	-0.233	-1.568	-0.869	0.122	3.163	-0.467	0.009	0.309	0.558	0.638
1.8	4.348	0.946	-0.233	-1.591	-0.883	0.125	3.037	-0.471	0.003	0.302	0.559	0.635
1.9	4.318	0.967	-0.228	-1.595	-0.881	0.125	-2.969	-0.476	-0.008	0.295	0.559	0.632
2	4.291	0.989	-0.225	-1.594	-0.880	0.125	-2.898	-0.489	-0.026	0.293	0.561	0.633
2.2	4.210	1.019	-0.219	-1.600	-0.879	0.126	-2.831	-0.535	-0.040	0.299	0.563	0.637
2.4	4.128	1.093	-0.221	-1.518	-0.880	0.113	-2.881	-0.561	-0.044	0.309	0.562	0.642
2.6	4.057	1.122	-0.205	-1.510	-0.875	0.111	-2.889	-0.568	-0.042	0.304	0.561	0.638
2.8	3.991	1.146	-0.186	-1.516	-0.870	0.112	-2.948	-0.548	-0.043	0.297	0.559	0.633
3	3.961	1.217	-0.171	-1.456	-0.860	0.101	3.256	-0.535	-0.054	0.287	0.561	0.630
3.5	3.875	1.314	-0.140	-1.372	-0.843	0.085	3.870	-0.534	-0.065	0.278	0.572	0.636
4	3.756	1.345	-0.114	-1.337	-0.819	0.081	4.006	-0.545	-0.076	0.271	0.570	0.631
4.5	3.657	1.367	-0.090	-1.303	-0.794	0.076	4.161	-0.556	-0.085	0.272	0.579	0.640
5	3.562	1.393	-0.070	-1.250	-0.770	0.068	4.262	-0.539	-0.081	0.274	0.592	0.652
5.5	3.479	1.407	-0.056	-1.221	-0.754	0.064	4.368	-0.526	-0.074	0.282	0.591	0.655
6	3.418	1.419	-0.049	-1.198	-0.742	0.060	4.403	-0.535	-0.084	0.288	0.590	0.657
6.5	3.394	1.451	-0.042	-1.140	-0.708	0.051	4.525	-0.558	-0.098	0.298	0.589	0.660
7	3.351	1.442	-0.039	-1.140	-0.677	0.052	4.494	-0.568	-0.103	0.306	0.586	0.661
7.5	3.293	1.403	-0.035	-1.190	-0.657	0.061	4.381	-0.564	-0.099	0.306	0.584	0.660
8	3.232	1.354	-0.030	-1.250	-0.641	0.072	4.266	-0.553	-0.090	0.305	0.580	0.655

Table 3 Results of the regression analyses on  $V_{EIR}$  obtained for different values of the SDOF period  $T$ 

$T[s]$	$a$	$b$	$c$	$d$	$e$	$f$	$h$	$m1$	$m2$	$\tau$	$\sigma$	$\sigma_T$
0.05	4.970	0.136	0.157	-2.233	0.034	0.148	11.085	-0.006	0.228	0.371	0.550	0.664
0.1	6.779	0.352	-0.127	-1.978	0.009	0.089	16.758	0.041	0.168	0.371	0.546	0.660
0.15	6.784	0.476	-0.133	-1.731	-0.089	0.069	15.798	0.030	0.168	0.314	0.513	0.602
0.2	6.108	0.733	-0.159	-1.217	-0.178	0.020	13.059	0.058	0.168	0.259	0.499	0.562
0.25	5.775	0.812	-0.176	-1.064	-0.284	0.011	10.777	0.017	0.175	0.234	0.489	0.542
0.3	5.456	0.802	-0.185	-1.018	-0.375	0.017	8.579	-0.055	0.211	0.228	0.492	0.542
0.35	5.421	0.782	-0.177	-1.076	-0.411	0.029	7.808	-0.110	0.179	0.209	0.493	0.536
0.4	5.448	0.719	-0.170	-1.235	-0.429	0.054	7.542	-0.112	0.166	0.223	0.492	0.540
0.45	5.396	0.683	-0.170	-1.337	-0.479	0.073	6.928	-0.141	0.144	0.234	0.497	0.549
0.5	5.364	0.658	-0.171	-1.417	-0.526	0.086	6.570	-0.177	0.145	0.220	0.504	0.550
0.55	5.259	0.628	-0.186	-1.479	-0.555	0.099	5.780	-0.191	0.154	0.215	0.516	0.559
0.6	5.176	0.602	-0.197	-1.548	-0.584	0.113	5.366	-0.188	0.165	0.227	0.523	0.570
0.65	5.029	0.602	-0.205	-1.554	-0.617	0.118	4.558	-0.180	0.188	0.235	0.529	0.578
0.7	4.925	0.597	-0.203	-1.566	-0.647	0.122	3.813	-0.196	0.218	0.236	0.531	0.581
0.75	4.888	0.608	-0.203	-1.569	-0.666	0.123	3.504	-0.210	0.215	0.233	0.529	0.578
0.8	4.838	0.619	-0.205	-1.574	-0.676	0.125	3.358	-0.196	0.208	0.236	0.525	0.576
0.85	4.820	0.621	-0.209	-1.599	-0.681	0.129	3.292	-0.194	0.201	0.240	0.528	0.580
0.9	4.819	0.612	-0.206	-1.641	-0.687	0.135	3.300	-0.194	0.206	0.252	0.533	0.589
0.95	4.832	0.594	-0.210	-1.701	-0.698	0.143	3.371	-0.208	0.194	0.263	0.535	0.596
1	4.837	0.577	-0.218	-1.760	-0.714	0.152	3.331	-0.221	0.184	0.271	0.535	0.599
1.1	4.790	0.571	-0.238	-1.816	-0.763	0.161	-3.052	-0.279	0.157	0.288	0.536	0.608
1.2	4.783	0.576	-0.245	-1.856	-0.766	0.167	-2.867	-0.301	0.141	0.297	0.535	0.612
1.3	4.761	0.616	-0.240	-1.843	-0.778	0.164	-3.015	-0.355	0.108	0.302	0.537	0.616
1.4	4.727	0.658	-0.227	-1.815	-0.797	0.158	-3.169	-0.400	0.100	0.299	0.535	0.613
1.5	4.708	0.684	-0.218	-1.795	-0.804	0.154	3.337	-0.432	0.093	0.295	0.536	0.612
1.6	4.670	0.699	-0.212	-1.794	-0.806	0.154	3.276	-0.428	0.077	0.292	0.540	0.613
1.7	4.615	0.706	-0.207	-1.808	-0.821	0.156	3.145	-0.407	0.069	0.290	0.542	0.615
1.8	4.584	0.700	-0.203	-1.848	-0.832	0.162	3.033	-0.404	0.071	0.282	0.542	0.611
1.9	4.581	0.699	-0.196	-1.875	-0.825	0.165	-2.983	-0.407	0.071	0.274	0.540	0.606
2	4.580	0.701	-0.192	-1.895	-0.821	0.167	-2.923	-0.417	0.062	0.272	0.542	0.606
2.2	4.549	0.693	-0.179	-1.942	-0.816	0.174	-2.844	-0.447	0.063	0.276	0.544	0.610
2.4	4.512	0.728	-0.174	-1.896	-0.809	0.166	-2.856	-0.454	0.080	0.284	0.545	0.615
2.6	4.470	0.726	-0.154	-1.913	-0.807	0.168	-2.845	-0.455	0.095	0.280	0.543	0.611
2.8	4.454	0.729	-0.134	-1.931	-0.796	0.169	-2.953	-0.438	0.107	0.273	0.541	0.606
3	4.469	0.773	-0.118	-1.887	-0.781	0.160	3.248	-0.421	0.104	0.261	0.542	0.601
3.5	4.481	0.814	-0.088	-1.859	-0.761	0.152	3.811	-0.394	0.105	0.241	0.550	0.600
4	4.455	0.813	-0.066	-1.858	-0.736	0.152	3.886	-0.382	0.103	0.230	0.547	0.593
4.5	4.446	0.810	-0.050	-1.849	-0.709	0.149	4.025	-0.379	0.103	0.227	0.554	0.599
5	4.417	0.816	-0.039	-1.820	-0.684	0.145	3.951	-0.356	0.110	0.227	0.563	0.607
5.5	4.382	0.811	-0.029	-1.811	-0.673	0.144	3.847	-0.342	0.121	0.231	0.562	0.607
6	4.360	0.814	-0.024	-1.788	-0.659	0.140	3.749	-0.342	0.119	0.235	0.558	0.606
6.5	4.366	0.826	-0.022	-1.750	-0.630	0.134	3.751	-0.355	0.117	0.242	0.554	0.605
7	4.364	0.805	-0.026	-1.762	-0.606	0.137	3.691	-0.361	0.118	0.247	0.549	0.602
7.5	4.359	0.773	-0.027	-1.796	-0.586	0.143	3.577	-0.358	0.125	0.246	0.544	0.597
8	4.351	0.728	-0.030	-1.846	-0.567	0.152	3.441	-0.352	0.133	0.243	0.540	0.592

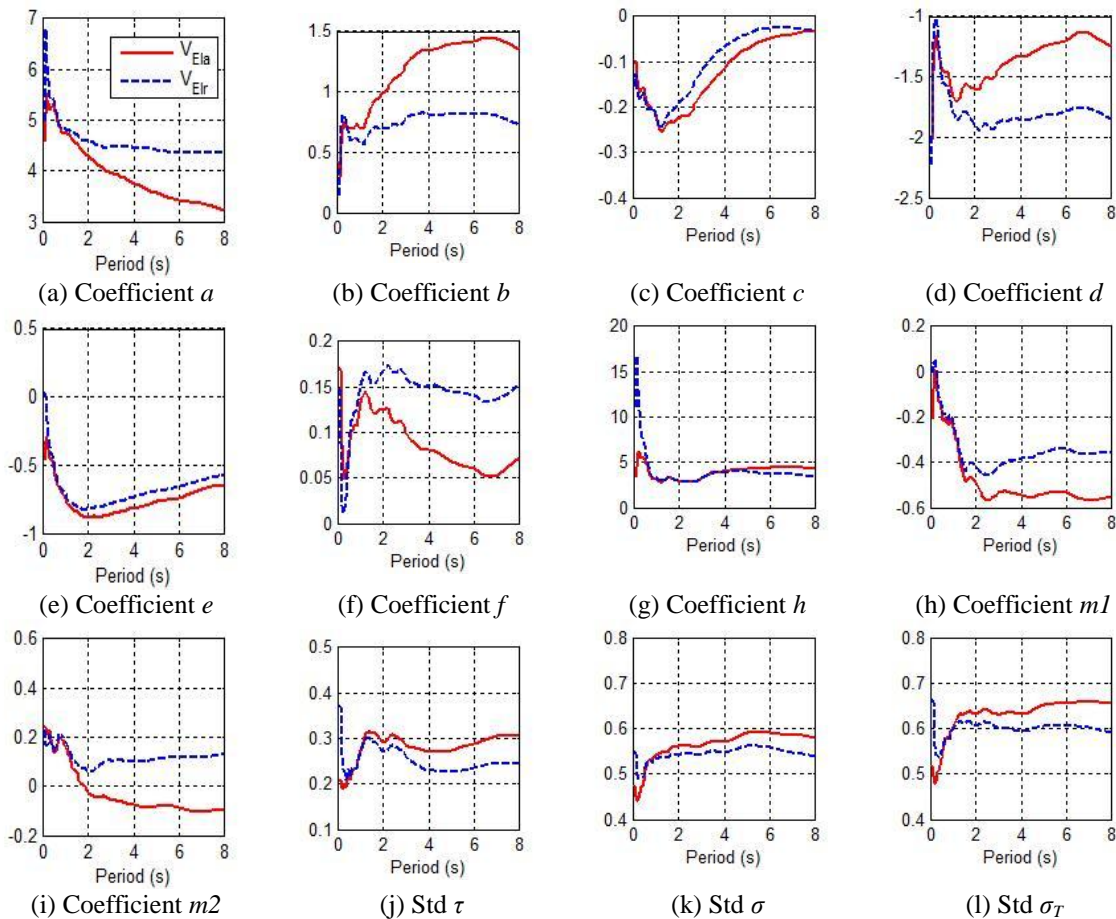


Fig. 7 Variation with period of the estimated model coefficients of the functional forms of  $V_{EIa}$  and  $V_{EIr}$ , and of the standard deviations of the error terms obtained in the regressions

### 6. Predicted $V_{EIa}$ and $V_{EIr}$ spectra

In Fig. 8,  $V_{EIa}$  and  $V_{EIr}$  spectra obtained with the proposed GMPEs for a strike-slip earthquake of 6.5 magnitude and a rupture distance equal to 30 km are reported. Spectra corresponding to different  $V_{S30}$  values show how soil condition affects these spectra. It is interesting to observe that while the intensity of  $V_{EIa}$  is always influenced by such variable,  $V_{EIr}$  does not depend on it at period values lower than 0.2s. In the same Figure, comparisons between spectra produced by different types of fault mechanism are also reported. The two velocities show the same trend. For both of them, in fact, the intensity produced by an earthquake with a strike-slip fault mechanism ranges in between the intensities corresponding to normal and reverse-faulting earthquakes. In particular, at short periods (lower than 0.2s, in the reported case) the velocity values produced by strike-slip and normal fault earthquakes are pretty the same; at large periods (higher than about 1.5s), the velocity values produced by the strike-slip fault earthquake converge toward those of the reverse fault earthquake.

In Figs. 9-10 the two velocity spectra are compared considering different distances and soil conditions, respectively. In this case it can be observed that while at short periods (lower than about 0.2s) the difference between the  $V_{Ela}$  and  $V_{EIr}$  value is large, with the increase of magnitude at periods higher than 1s the difference reduces.

In order to clearly show differences in the intensity of the two velocities, the variation of the  $V_{Ela}$  to  $V_{EIr}$  ratio with distance is reported in Fig. 11 considering a strike-slip fault earthquake, and a  $V_{S30}$  value equal to 525 m/s. The most significant difference in the values of the two velocities can be observed at large periods and short distances for  $M=5$ , and short periods and large distances for  $M=8$ . For a period value equal to 1s, the  $V_{Ela}$  to  $V_{EIr}$  ratio is always around 1, while at periods much larger or lower than 1s is more sensitive to distance. With the increase of magnitude, however, all the  $V_{Ela}$  to  $V_{EIr}$  ratio values, except that corresponding to 0.2s (the red curve), approach 1. It is interesting to note that the curve corresponding to a T value equal to 0.2s is characterized by an inflection point at a distance of 15 km circa, with a difference between the slope of the curve before and after this point which increases with the increase of magnitude. A similar trend has been also observed by Chapman (1999), but for the  $V_{Ela}$  to PSV (pseudo-velocity spectrum) ratio. The inflection is due to the difference in the value of  $h$  estimated for  $V_{Ela}$  and  $V_{EIr}$  at short periods. It is important to underline that  $h$  is not true focal depth, but simply a model parameter used in the functional form to represent the flattening of attenuation observed at small distances, especially for  $V_{EIr}$  at short periods.

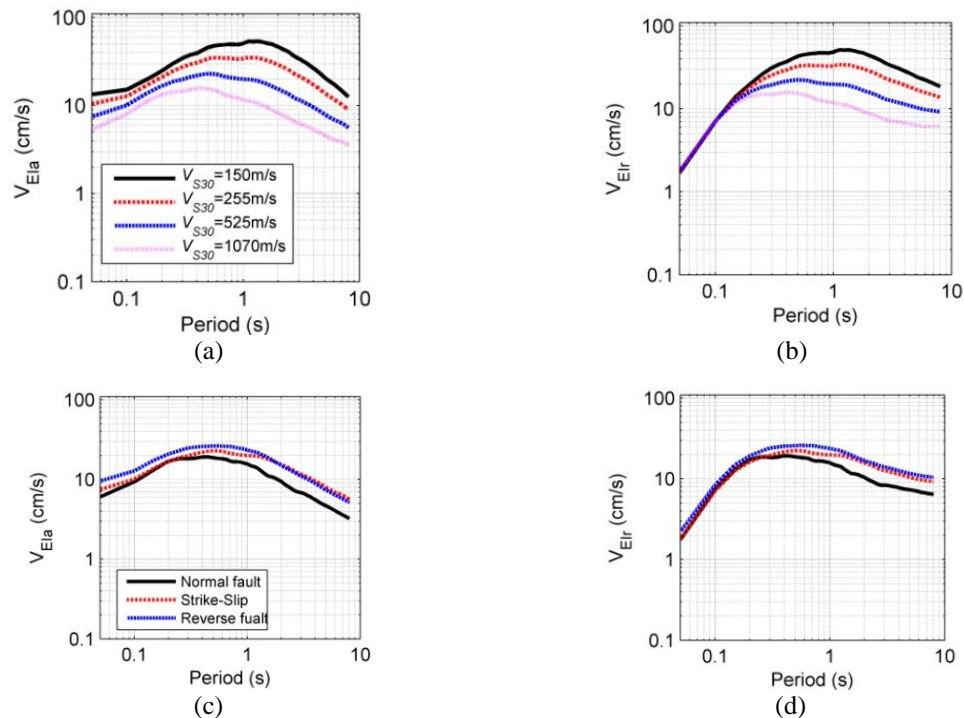


Fig. 8 Predicted  $V_{Ela}$  and  $V_{EIr}$  spectra for magnitude  $M=6.5$  and distance  $R=30$  km considering: different  $V_{S30}$  values (corresponding to different NEHRP soil conditions) for the same strike-slip fault mechanism (plots a and b), and different fault mechanisms for  $V_{S30}=525$  m/s (plots c and d)

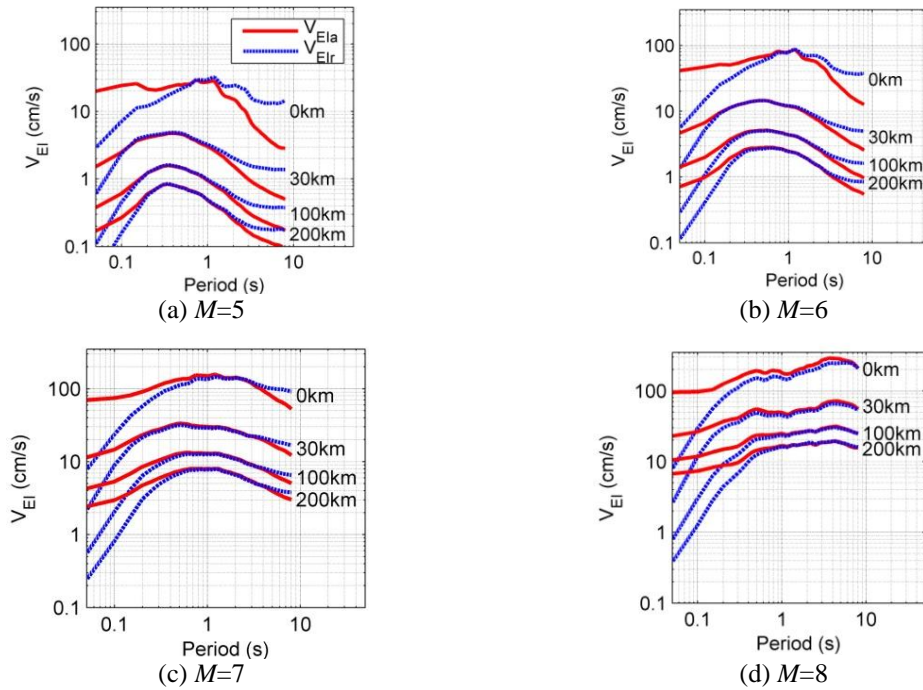


Fig. 9 Comparison between  $V_{EIa}$  and  $V_{EIr}$  spectra produced by a strike-slip earthquake, a  $V_{S30}$  equal to 525 m/s (corresponding to a soil type C, according to NEHRP classification), and various distance and magnitude values

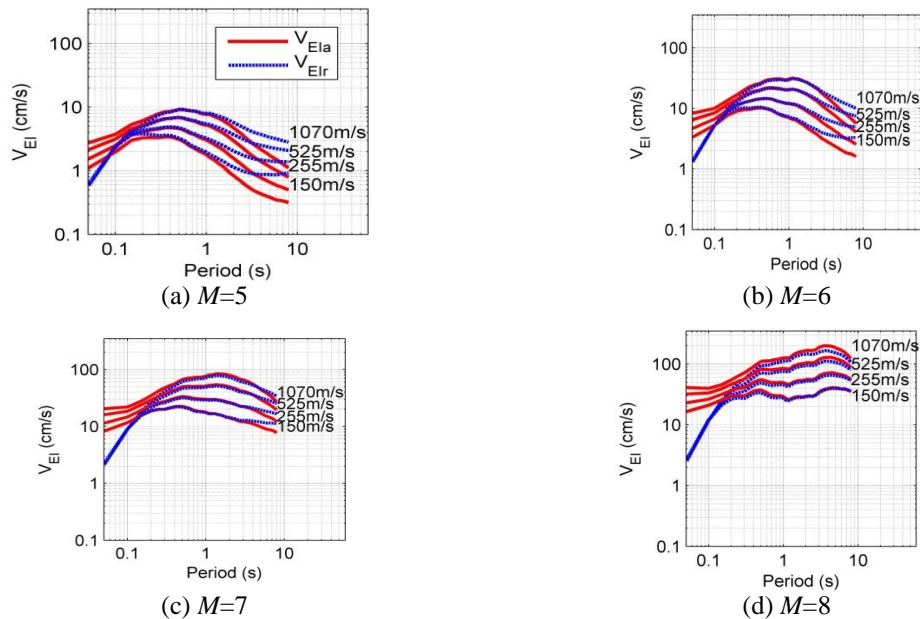


Fig. 10 Comparison between  $V_{EIa}$  and  $V_{EIr}$  spectra produced by a strike-slip earthquake, a distance equal to 30km, and various  $V_{S30}$  and magnitude values

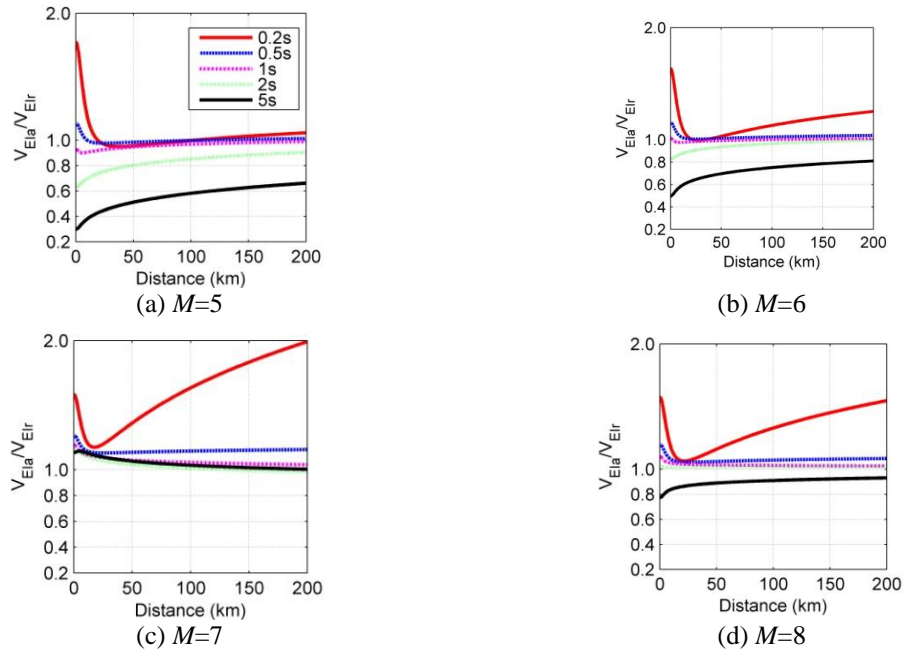


Fig. 11  $V_{EIa}$  to  $V_{EIr}$  ratio vs distance (closest distance to the fault) calculated for a strike-slip earthquake with  $V_{S30}=525$  m/s considering different magnitude and oscillator period values

## 7. Comparison with models from the literature

In this section of the paper, input energy spectra obtained with the proposed GMPEs and models from the literature are compared. The prediction equations selected from the literature are those of Chapman (1999), Danciu and Tselentis (2007), and Gong and Xie (2005). The following different magnitude and source-to-site distance values are considered in the comparisons:  $M$  equal to 6 and 7, and  $R$  equal to 5, 30, 60 and 120 km. These values are consistent with the range of applicability of the prediction equations selected from the literature. The type of fault considered is the reverse. Although in Chapman (1999) and Gong and Xie (2005) fault mechanism effects are not accounted for, the records used to develop their prediction equations are dominated by reverse fault earthquakes, especially at magnitudes equal to 6 (e.g., dominated by Whittier 10/1/1987) and 7 (e.g., dominated by Northridge 1/17/1994 and Loma Prieta 10/18/1989). Since the prediction equations from the literature use different distance measures than the closest distance to rupture  $R$  considered in this study, a conversion is needed. The equations of Kaklamanos *et al.* (2011) are applied to convert  $R$  to the Joyner-Boore distance  $R_{JB}$ , that is, the closest distance to the surface projection of the fault rupture.  $R_{JB}$  is used in Chapman (1999) and Gong and Xie (2005), and can be considered a quite good approximation of the epicentral distance (Kaklamanos *et al.* 2011) which is used in Danciu and Tselentis (2007). It should be noted that while the difference between these distance measures is significant in the near source region, it becomes negligible far from the field. The last comment before discussing the results of the comparisons is about the different definitions used in the prediction equations for the input energy spectra. In Chapman (1999), Gong and Xie (2005) and the present study, each ordinate of the spectra is the geometric mean of the

input energy equivalent velocities obtained for the two horizontal components of the ground motion, in Danciu and Tselentis (2007), instead, is the arithmetic mean. In the present study, the geometric mean was preferred to other combination rules because in seismic risk calculations its use makes easy to link probabilistic seismic demand models (where the logarithm of the response parameter is commonly expressed in terms of the logarithm of the considered IM) and seismic hazard analyses.

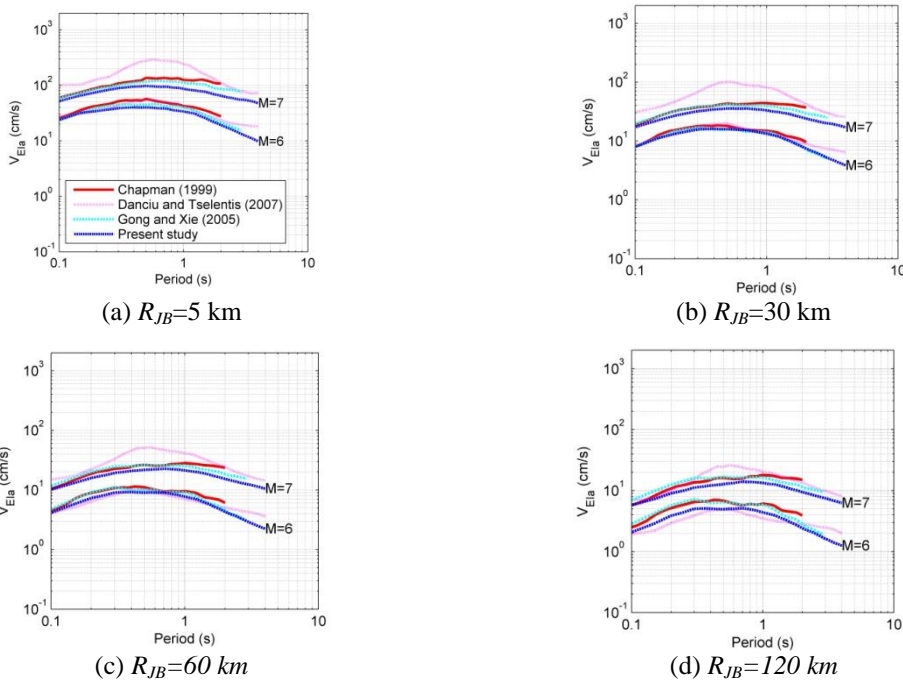


Fig. 12  $V_{Ela}$  spectra predicted for different magnitude and Joyner-Boore distance values, corresponding to an earthquake with a reverse fault mechanism and a soil condition of NEHRP type B (modelled with a  $V_{S30}$  equal to 525m/s)

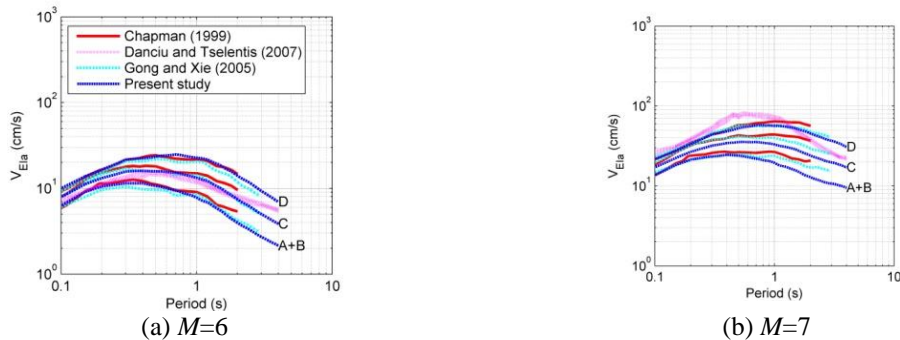


Fig. 13  $V_{Ela}$  spectra predicted for different types of soil (NEHRP A+B, C, and D modelled with  $V_{S30}$  equals to 1070m/s, 525m/s, and 255m/s, respectively), corresponding to an earthquake with a reverse fault mechanism and a Joyner-Boore distance equal to 30km

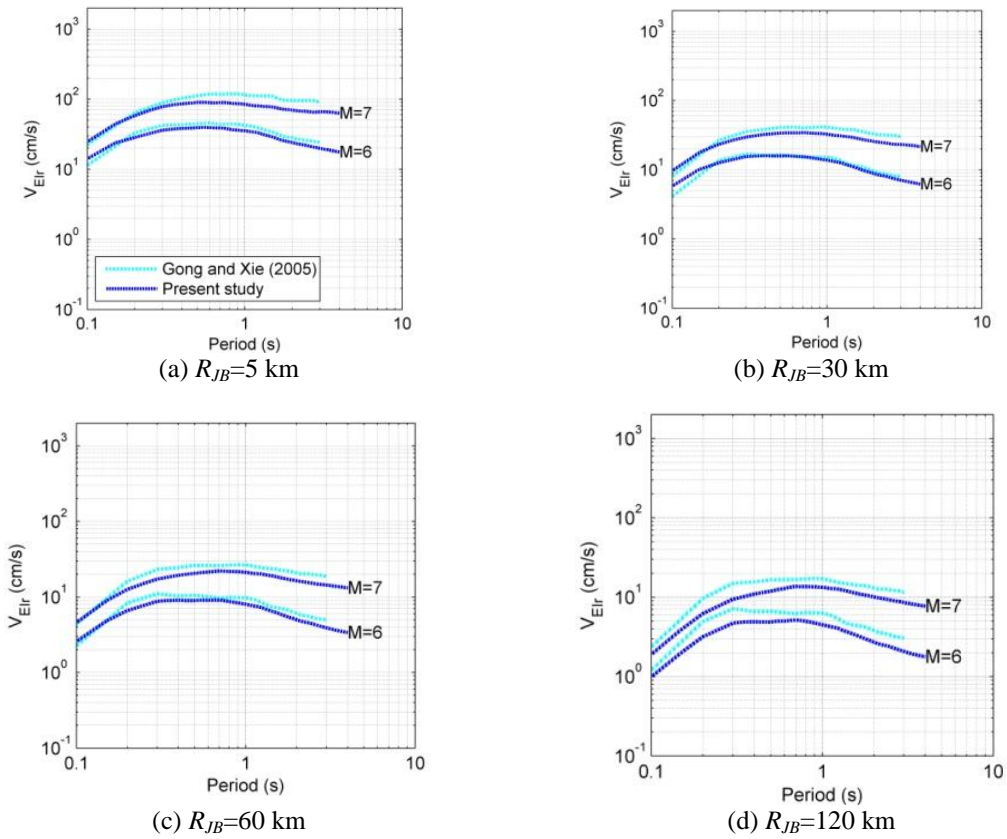


Fig. 14  $V_{EIr}$  spectra predicted for different magnitude and Joyner-Boore distance values, corresponding to an earthquake with a reverse fault mechanism and a soil condition of NEHRP type B (modelled with a  $V_{S30}$  equal to 525m/s)

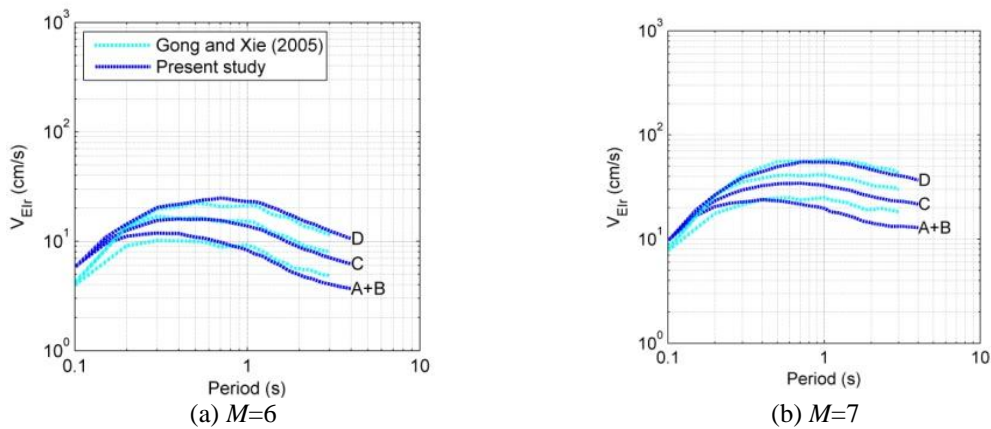


Fig. 15  $V_{EIr}$  spectra predicted for different types of soil (NEHRP A+B, C, and D modelled with  $V_{S30}$  equals to 1070m/s, 525m/s, and 255m/s, respectively), corresponding to an earthquake with a reverse fault mechanism and a Joyner-Boore distance equal to 30km

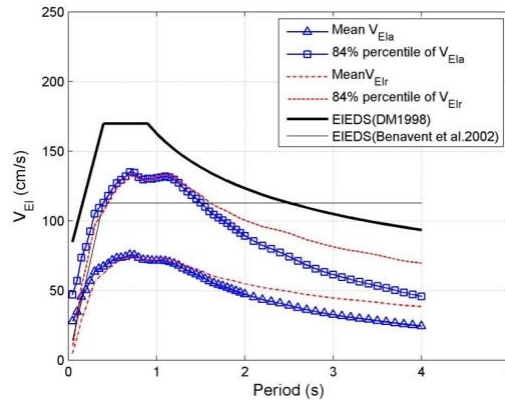


Fig. 16 Comparison of input energy spectra proposed in this study with Elastic Input Energy Design Spectra (EIEDS,  $M=6.2$ , distance= 10 km and  $V_{s30} = 250$  m/s) proposed in Decanini and Mollaioli 1998 (DM1998,  $5.4 < M < 6.2$ , soil S2 and  $5 < D_f < 12$  km) and in Benavent *et al.* 2002 (PGA=0.23g,  $T_g=0.40$  and  $K=1$ , corresponding to a moderate earthquake with magnitude in the same interval of Decanini and Mollaioli 1998 and a return period of 475 years).

In Fig. 12,  $V_{Ela}$  spectra corresponding to different magnitude and distance values are plotted. The most significant discrepancy in the predictions can be observed between the spectra obtained with Danciu and Tselentis (2007) and those obtained with the other three GMPEs when the magnitude is equal to 7. This is probably due to the fact that in Danciu and Tselentis (2007) the magnitude saturation phenomenon is not explicitly taken into account, as it is in the other prediction equations which use a nonlinear magnitude scaling term in addition to a linear one. This may lead to an overestimation of  $V_{Ela}$  with the increase of magnitude. Differences between the spectra obtained with Chapman (1999) and the proposed GMPE can be observed at period values higher than about 0.6s. However, compared to both Chapman (1999) and Gong and Xie (2005), the proposed GMPE produces in general comparable spectra which become very similar for the case of magnitude 6 and distance equal to 30 km. This consistency in the predictions can be due to the large number of data used in the regression for this earthquake scenario.

In Fig.13,  $V_{Ela}$  spectra corresponding to different soil conditions are shown. It can be noted that for the considered case studies using Danciu and Tselentis (2007) the predicted spectra do not significantly change with the type of soil. On the contrary, soil conditions clearly affect the spectra obtained with the other prediction equations, with the  $V_{Ela}$  values being almost the same at short periods. The most significant difference between the results obtained with the proposed GMPE and those of Chapman (1999) and Gong and Xie (2005) can be found for the case of soil type A+B and magnitude equal to 7. This can be due both to the lack of soil type A+B records in the databases used by Chapman (1999) and Gong and Xie (2005), and to the fact that they used different parameters (dummy variables instead of  $V_{s30}$ ) with respect to the present study to account for the soil effects.

Danciu and Tselentis (2007) predictive equations for  $V_{EIr}$  are not developed, Gong and Xie (2005) only is used in the evaluation of the proposed GMPE. In these Figures, the same types of comparisons shown for  $V_{Ela}$  are reported and similar trends can be observed. In particular, by

looking at the plots of Fig. 14 it can be stated that the spectra predicted with the two GMPEs are very similar, especially for the case of magnitude 6 and distance equal to 30 km. The effects of soil condition, shown in the plots of Fig. 15, are very similar except for the case of soil type A+B and magnitude equal to 7. Also in this case, the same explanations of those proposed for  $V_{Ela}$  can be given.

Finally, in Fig.16 a comparison of with the proposals of Decanini and Mollaioli 1998 and Benavent-Climent *et al.* 2002 (Benavent *et al.* 2002) is presented. It is possible to observe that the spectral shapes of  $V_{EIr}$  and  $V_{Ela}$  proposed in this study are comparable with that proposed by Decanini and Mollaioli (1998). The elastic input energy design spectrum proposed by Decanini and Mollaioli (1998) is evidently larger of the median  $V_{EIr+1sigma}$  (84% percentile of  $V_{EIr}$ ) and the median  $V_{Ela+1sigma}$  (84% percentile of  $V_{Ela}$ ) for its conservative feature.

The input energy design spectra proposed by Benavent-Climent *et al.* 2002 is encompassed between the median and median+1sigma input energy spectra proposed in this study in the period range of 0.4s-1.5s. In the medium and long period ranges by assuming a horizontal segment for the design spectrum, the proposal of Benavent-Climent *et al.* (2002) might seem too conservative. However, it should be noted in this case that it is due to a quite small number of records available and therefore it was considered advisable to adopt a constant branch of the design spectrum.

## 8. Summary and conclusion

Studies have shown that in order to predict the seismic response of structures the absolute input energy equivalent velocity  $V_{Ela}$  and the relative input energy equivalent velocity  $V_{EIr}$  can be considered in some cases as good alternatives with respect to standard intensity measures commonly used in performance-based earthquake engineering, such as the peak ground acceleration or the pseudo-spectral acceleration.  $V_{Ela}$  and  $V_{EIr}$ , in fact, are intensity measures that are able to capture not only the duration and amplitude of the ground motion but also the dynamic properties of the structure.

In the present work, empirical ground motion prediction equations developed based on a mixed-effect model are proposed for estimating both  $V_{Ela}$  and  $V_{EIr}$ . The model coefficients have been calibrated through regression analyses using records selected from the NGA database. The proposed equations can be applied to predict  $V_{Ela}$  and  $V_{EIr}$  for shallow crustal earthquakes occurring in active tectonic region, with a magnitude range of 5 to 8, a distance less than 200 km, and a  $V_{S30}$  value in the range of 150-1500m/s.

The improvements with respect to prediction equations for input energy spectra already available from the literature can be identified in the following: the proposed equations have been developed using a large number of records characterized by a wide range of magnitude and distance values; they include a  $V_{S30}$  term that enables to better evaluate the effects of soil conditions than simple dummy variables; they also include terms to explicitly account for different types of fault mechanisms; a prediction equation for the relative input energy equivalent velocity, intensity measure that has been not still received much research attention, has been also proposed.

By using the proposed prediction equations, the effects on  $V_{Ela}$  and  $V_{EIr}$  of earthquake magnitude, fault type, source-to-site distance and soil condition variation have been investigated. Comparisons between predictions obtained with the proposed equations and with others from the literature have been shown and discussed.

## Acknowledgments

The financial support of both the Italian Ministry of the Instruction, University and Research (MIUR) and the Italian Network of University Laboratories of Seismic Engineering (ReLuis) is gratefully acknowledged.

## References

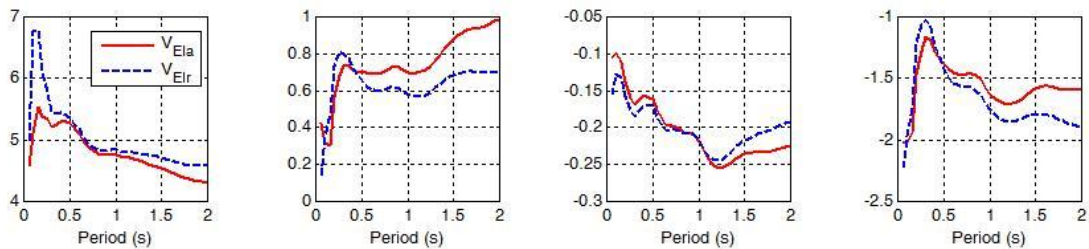
- Abrahamson, N. and Silva, W. (2008), "Summary of the Abrahamson & Silva NGA ground-motion relations", *Earthq. Spectra*, **24**(1), 67-97.
- Abrahamson, N.A. and Youngs, R.R. (1992), "A stable algorithm for regression analyses using the random effects model", *Bull. Seismol. Soc. Am.*, **82**(1), 505-510.
- Akiyama, H. (1985), *Earthquake-Resistant Limit-State Design for Buildings*. University of Tokyo Press.
- Benavent-Climent, A., Pujades, L.G. and Lopez-Almansa, F. (2002), "Design energy input spectra for moderate-seismicity regions", *Earthq. Eng. Struct. Dyn.*, 2002, **31**, 1151-1172.
- Benavent-Climent, A., Lopez-Almansa, F. and Bravo-Gonzalez, D.A. (2010a), "Design energy input spectra for moderate-to-high seismicity regions based on Colombian earthquakes", *Soil. Dyn. Earthq. Eng.*, **30**(11), 1129-1148.
- Benavent-Climent, A. and Zahran R. (2010b), "Seismic evaluation of existing RC frames with wide beams using an energy-based approach", *Earthq. Struct.*, **1**(1), 93-108.
- Boore, D.M., Atkinson, G.M. (2008), "Ground-motion prediction equations for the average horizontal component of pga, pgv, and 5%-damped psa at spectral periods between 0.01 s and 10.0 s", *Earthq. Spectra*, **24**(1), 99-138.
- Boore, D.M., Joyner, W.B. and Fumal, T.E. (1993), "Estimation of response spectra and peak accelerations from western North American earthquakes: An interim report", U. S. Geological Survey Open-File Report 93-509
- Brillinger, D.R. and Preisler, H.K. (1984), "An exploratory analysis of the Joyner-Boore attenuation data", *Bull. Seismol. Soc. Am.*, **74**(4), 1441-1450.
- Brillinger, D.R. and Preisler, H.K. (1985), "Further analysis of the Joyner-Boore attenuation data", *Bull. Seismol. Soc. Am.*, **75**(2), 611-614.
- Campbell, K.W., Bozorgnia, Y. (2008), "NGA ground motion model for the geometric mean horizontal component of pga, pgv, pgd and 5% damped linear elastic response spectra for periods ranging from 0.01 to 10 s", *Earthq. Spectra*, **24**(1), 139-171.
- Chapman, M.C. (1999), "On the use of elastic input energy for seismic hazard analysis", *Earthq. Spectra*, **15**(4), 607-635.
- Chiou, B.J. and Youngs, R.R. (2008), "An NGA model for the average horizontal component of peak ground motion and response spectra", *Earthq. Spectra*, **24**(1), 173-215.
- Danciu, L. and Tselentis, G.A. (2007), "Engineering ground-motion parameters attenuation relationships for Greece", *Bull. Seismol. Soc. Am.*, **97**(1), 162-183.
- Decanini, L. and Mollaioli, F. (1998), "Formulation of elastic earthquake input energy spectra", *Earthq. Eng. Struct. Dyn.*, **27**(13), 1503-1522.
- Decanini, L. and Mollaioli, F. (2001), "An energy-based methodology for the assessment of seismic demand", *Soil. Dyn. Earthq. Eng.*, **21**(2), 113-137.
- Fajfar, P. and Fischinger, M. (1990), "A seismic procedure including energy concept", 9th European Conference on Earthquake Engineering, Moscow, September, vol. 2, 312-321.
- Foulser-Piggott, R. and Stafford, P.J. (2012), "A predictive model for arias intensity at multiple sites and consideration of spatial correlations", *Earthq. Eng. Struct. Dyn.*, **41**(3), 431-451.
- Gong, M.S. and Xie, L.L. (2005), "Study on comparison between absolute and relative input energy spectra

- and effects of ductility factor”, *Acta. Seismol. Sin.*, **18**(6), 717-726.
- Idriss, I. (2008), “An empirical model for estimating the horizontal spectral values generated by shallow crustal earthquakes”, *Earthq. Spectra*, **24**(1), 217-242.
- Jayaram, N., Mollaioli, F., Bazzurro, P., De Sortis, A. and Bruno, S. (2010), “Prediction of structural response in reinforced concrete frames subjected to earthquake ground motions”, *Proceeding of the 9th US National and 10th Canadian Conference on Earthquake Engineering*, Oakland, Canada, July.
- Kaklamanos, J., Baise, L.G. and Boore, D.M. (2011), “Estimating unknown input parameters when implementing the NGA ground-motion prediction equations in engineering practice”, *Earthq. Spectra*, **27**(4), 1219-1235.
- Kalkan, E. and Kunnath, S.K. (2008), “Relevance of absolute and relative energy content in seismic evaluation of structures”, *Adv. Struct. Eng.*, **11**(1), 17-34.
- López-Almansa, F., Yazgan, A., Benavent-Climent, A. (2013), “Design energy input spectra for high seismicity regions based on Turkish registers”, *Bull. Earthq. Eng.*, **11**(4), 885-912.
- Lucchini, A., Cheng, Y., Mollaioli, F. and Liberatore, L. (2013), “Predicting floor response spectra for rc frame structures”, *4th ECCOMAS Thematic Conference on Computational Methods in Structural Dynamics and Earthquake Engineering*, Kos, Greece, June.
- Lucchini, A., Mollaioli, F. and Monti, G. (2011), “Intensity measures for response prediction of a torsional building subjected to bi-directional earthquake ground motion”, *Bull. Earthq. Eng.*, **9**(5), 1499-1518.
- Luco, N., Manuel, L., Baldava, S. and Bazzurro, P. (2005), “Correlation of damage of steel moment-resisting frames to a vector-valued ground motion parameter set that includes energy demands”, *USGS Award 03HQGR0057-03HQGR0106*, Final Report.
- Manfredi, G. (2001), “Evaluation of seismic energy demand”, *Earthq. Eng. Struct. Dyn.*, **30**(4), 485-499.
- Mollaioli, F., Bruno, S., Decanini, L. and Saragoni, R. (2011), “Correlations between energy and displacement demands for performance-based seismic engineering”, *Pure Appl. Geophys.*, **168**(1-2), 237-259.
- Mollaioli, F., Lucchini, A., Cheng, Y. and Monti, G. (2013), “Intensity measures for the seismic response prediction of base-isolated buildings”, *Bull. Earthq. Eng.*, **11**(5), 1841-1866.
- Özbeç, C., Sari, A., Manuel, L., Erdik, M. and Fahjan, Y. (2004), “An empirical attenuation relationship for northwestern turkey ground motion using a random effects approach”, *Soil. Dyn. Earthq. Eng.*, **24**(2), 115-125.
- Pinheiro, J., Bates, D., DebRoy, S. and Sarkar, D. (2007), *Linear and nonlinear mixed effects models*. R package version 3:57
- Rezaeian, S., Bozorgnia, Y., Idriss, I.M., Campbell, K., Abrahamson, N. and Silva, W. (2012), “Spectral damping scaling factors for shallow crustal earthquakes in active tectonic regions”, *PEER Report 2012/01*, Pacific Earthquake Engineering Research Center, University of California, Berkeley.
- Somerville, P.G., Smith, N.F., Graves, R.W. and Abrahamson, N.A. (1997), “Modification of empirical strong ground motion attenuation relations to include the amplitude and duration effects of rupture directivity”, *Seismol. Res. Lett.*, **68**(1), 199-222.
- Takewaki, I. (2004), “Bound of earthquake input energy”, *J. Struct. Eng.*, **130**(9), 1289-1297.
- Takewaki, I. and Tsujimoto, H. (2011), “Scaling of design earthquake ground motions for tall buildings based on drift and input energy demands”, *Earthq. Struct.*, **2**(2), 171-187.
- Uang, C.M. and Bertero, V.V. (1990), “Evaluation of seismic energy in structures”, *Earthq. Eng. Struct. Dyn.*, **19**(1), 77-90.
- Yakut, A. and Yilmaz, H. (2008), “Correlation of deformation demands with ground motion intensity”, *J. struct. Eng.*, **134**(12), 1818-1828.

**Appendix**

Table A. Symbols and acronyms used in this study

Symbol or acronym	Meaning
PGA	Peak ground acceleration
PGV	Peak ground velocity
PGD	Peak ground displacement
$S_a$	Pseudo-spectral acceleration
IM	Intensity measure
EDP	Engineering demand parameter
GMPE	Ground motion prediction equation
PSHA	Probabilistic seismic hazard analysis
PSDA	Probabilistic Seismic Demand Analysis
NGA	Next Generation Attenuation
PBEE	Performance-based earthquake engineering
$V_{S30}$	average shear-wave velocity within 0-30 meters depth
SDOF	Single degree of freedom
$M$	Magnitude
$R$	Closest distance to rupture
$R_{JB}$	Joyner-Boore distance
$E_{Ia}$	Absolute input energy
$E_{Ir}$	Relative input energy
$V_{EIa}$	Absolute input energy equivalent velocity
$V_{EIr}$	Relative input energy equivalent velocity
NLME	Nonlinear mixed effects model
NEHRP	National Earthquake Hazards Reduction Program
PSV	Pseudo spectral velocity
SS,R,RO, N, NO	Strike-slip fault, Reverse fault, Reverse-oblique fault, Reverse-oblique fault, and Normal-oblique fault, respectively
A	NEHRP site class A
B	NEHRP site class B
C	NEHRP site class C
D	NEHRP site class D
E	NEHRP site class E



(a) Coefficient  $a$  (b) Coefficient  $b$  (c) Coefficient  $c$  (d) Coefficient  $d$   
 Fig. A Variation of the estimated model coefficients of the functional forms of  $V_{EIa}$  and  $V_{EIr}$  with period from 0-2s

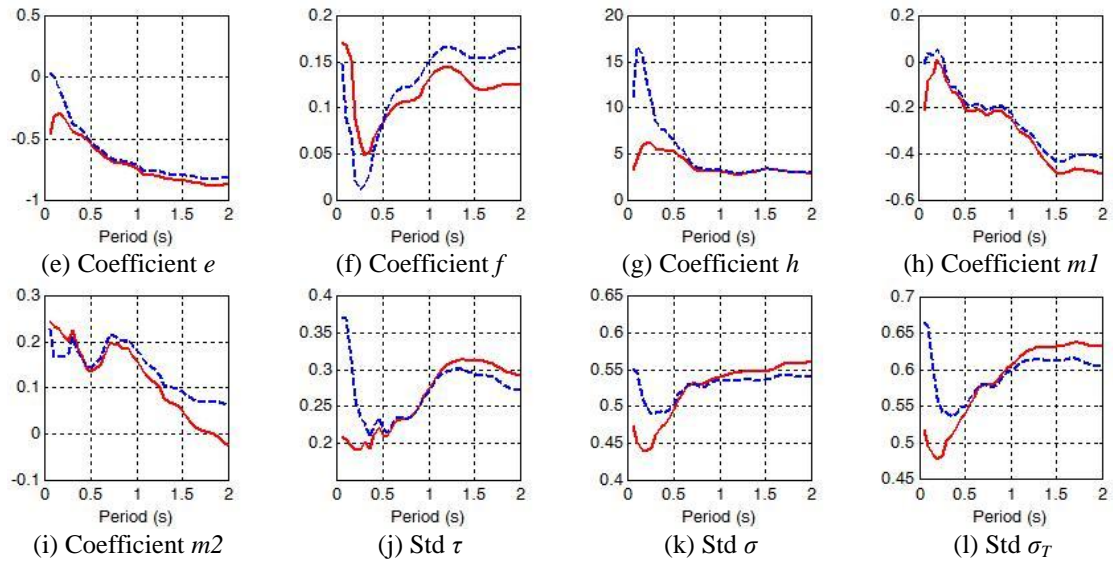


Fig. A Continued